CEACAM5-Targeted Immuno-PET in Androgen Receptor–Negative Prostate Cancer

Cinzia Imberti*[1], Roberto De Gregorio*[1], Joshua A. Korsen[1,2], Tran T. Hoang[1,2], Samantha Khitrov[1], Teja Kalidindi[1], Subhiksha Nandakumar[3], Jooyoung Park[4], Samir Zaidi[5,6], Naga Vara Kishore Pillarsetty[1,7], and Jason S. Lewis[1,2,7,8]

[1]Department of Radiology, Memorial Sloan Kettering Cancer Center, New York, New York; [2]Department of Pharmacology, Weill Cornell Medicine, New York, New York; [3]Department of Epidemiology and Biostatistics, Memorial Sloan Kettering Cancer Center, New York, New York; [4]Department of Biomedical Sciences, Korea University College of Medicine, Seoul, Korea; [5]Department of Genitourinary Oncology, Memorial Sloan Kettering Cancer Center, New York, New York; [6]Human Oncology and Pathogenesis Program, Memorial Sloan Kettering Cancer Center, New York, New York; [7]Department of Radiology, Weill Cornell Medicine, New York, New York; and [8]Molecular Pharmacology Program, Memorial Sloan Kettering Cancer Center, New York, New York

The incidence of androgen receptor (AR)–negative (AR^-) prostate cancer, including aggressive neuroendocrine prostate cancer (NEPC), has more than doubled in the last decade, but its timely diagnosis is difficult as it lacks typical prostate cancer hallmarks. The carcinoembryonic antigen–related cell adhesion molecule 5 (CEACAM5) has recently been identified as an upregulated surface antigen in NEPC. We developed an immuno-PET agent targeting CEACAM5 and evaluated its ability to delineate AR^- prostate cancer in vivo. **Methods:** CEACAM5 expression was evaluated in a panel of prostate cancer cell lines by immunohistochemistry and Western blotting. The CEACAM5-targeting antibody labetuzumab was conjugated with the chelator desferrioxamine (DFO) and radiolabeled with ^{89}Zr. The in vivo distribution of the radiolabeled antibody was evaluated in xenograft prostate cancer models by PET imaging and ex vivo organ distribution. **Results:** The NEPC cell line H660 exhibited strong CEACAM5 expression, whereas expression was limited in the AR^- cell lines PC3 and DU145 and absent in the AR–positive cell line LNCaP. [^{89}Zr]Zr-DFO-labetuzumab imaging was able to clearly delineate both neuroendocrine H660 xenografts and AR^- DU145 in vivo but could not detect the AR–positive xenograft LNCaP. **Conclusion:** Immuno-PET imaging with [^{89}Zr]Zr-DFO-labetuzumab is a promising diagnostic tool for AR^- prostate cancer.

Key Words: CEACAM5; androgen receptor–negative prostate cancer; immuno-PET; molecular imaging

J Nucl Med 2024; 65:1043–1050
DOI: 10.2967/jnumed.123.267107

Prostate cancer is one of the most common types of cancer and the second leading cause of cancer-related deaths in men in the United States (*1*). Androgen receptor (AR)–dependent prostate cancer is the most frequent and most studied form of prostate cancer. Accordingly, AR–dependent prostate cancer management has seen significant improvement in recent years (*2*), with androgen deprivation therapy becoming the standard of care and several diagnostic biomarkers being identified, including prostate-specific antigen, prostate stem cell antigen, and prostate-specific membrane antigen (PSMA) (*3*). However, the incidence of AR–negative (AR^-) prostate cancer has greatly increased in the last few decades. This can be partly attributed to the selection pressure of androgen deprivation therapy, which can drive the emergence of AR^- cancer cells. Consequently, the percentage of patients with metastatic castration-resistant prostate cancer displaying an AR^- profile has increased from 11.7% in 1998–2011 to 36.6% in 2012–2016 (*2,4*). AR^- prostate cancers are not only hard to treat, being generally resistant to standard prostate cancer therapies, but also difficult to detect, since they lack typical AR–dependent prostate cancer diagnostic biomarkers such as PSMA and prostate stem cell antigen. Research into new diagnostic agents for AR^- prostate cancer is critical for timely diagnosis and treatment decisions, enabling earlier patient enrollment in clinical trials or initiation of chemotherapy as necessary.

A particularly aggressive form of treatment-related AR^- prostate cancer is neuroendocrine prostate cancer (NEPC), which arises because of the lineage plasticity of prostate cancer cells, resulting in neuroendocrine differentiation with loss of AR expression and acquisition of neuroendocrine markers such as chromogranin A, synaptophysin, and CD56 (also known as NCAM) (*5*). The δ-like ligand 3 has recently been recognized as an NEPC-specific biomarker, and we showed that ^{89}Zr-labeled δ-like ligand 3–targeting antibodies could selectively detect NEPC using PET (*6*) and that a ^{177}Lu-labeled version of the same antibody was effective in NEPC-targeted radiotherapy (*7*).

Recently, an integrated transcriptomic and cell-surface proteomic approach has identified the carcinoembryonic antigen–related cell adhesion molecule 5 (CEACAM5), also known as CEA or CD66e, as an upregulated antigen in a large subset of NEPC cell lines, patient-derived xenografts, and patient tumors (*8*). Elevated CEACAM5 serum levels in castration-resistant prostate cancer patients have previously been associated with aggressive disease and poor prognosis (*9*).

CEACAM5 is a member of the CEACAM family, a group of cell surface glycoproteins belonging to the superfamily of immunoglobulin cell adhesion molecules (*10,11*). It has 7 glycosylated extracellular immunoglobulin domains, including 1 variable-like domain (N domain) and 3 repeating units (A1B1, A2B2, and A3B3) comprising 6 constant C2-like domains. CEACAM5 is anchored to the cell membrane at the B3 domain through a

Received Jan. 3, 2024; revision accepted Apr. 13, 2024.
For correspondence or reprints, contact Naga Vara Kishore Pillarsetty (pillarsn@mskcc.org) or Jason S. Lewis (lewisj2@mskcc.org).
*Contributed equally to this work.
Published online May 23, 2024.

glycosylated phosphatidylinositol moiety. The most external domain is the N terminus, which plays a major role in cell–cell adhesion (*12*). CEACAM5 is overexpressed in several types of cancer, whereas distribution in normal tissue is limited mostly to the apical surface of the gastrointestinal epithelium and other mucosal epithelial cells. It was first recognized as a tumor-associated antigen in colorectal cancer (*13*) in the mid-1960s and was used both as a serum marker for this disease (because colon cancer cells continuously exfoliate membrane components into the bloodstream) and as a target for antibody-based imaging of colorectal cancer (*14*). A recently completed clinical trial (NCT00645060) investigated the use of a ^{90}Y humanized anti-CEACAM5 antibody, M5A, in patients with CEACAM5-producing cancers (including colorectal cancer, non–small cell lung cancer, breast cancer, and medullary thyroid cancer) (*15*). An ^{225}Ac version of the same antibody is currently in a clinical trial for α-radiotherapy of CEACAM5-expressing cancers (NCT05204147), whereas M5A antibodies labeled with ^{64}Cu and ^{124}I are being clinically investigated as PET diagnostic tools (NCT02293954 and NCT03993327). More recently, a CEACAM5-targeting ^{68}Ga single-domain antibody has been evaluated in colorectal cancer patients (*16*). Labetuzumab govitecan, an antibody–drug conjugate of a humanized anti-CEACAM5 antibody binding to CEACAM5 A3B3 epitope (labetuzumab) with the topoisomerase inhibitor SN-38, has been used for treatment-refractory metastatic colorectal cancer (*17*).

The recent identification of CEACAM5 as a potential marker for NEPC has paved the way for CEACAM5-targeted therapies to be investigated in prostate cancer. Labetuzumab govitecan was shown to eradicate CEACAM5-positive NEPC xenografts and patient-derived xenograft models (*18*). CEACAM5-targeting CAR-T cells encoding a single-chain variable fragment derived from either labetuzumab or the fully human monoclonal antibody 1G9 have also been developed and tested preclinically in NEPC models (*8,19*).

In this work, we explored the potential of CEACAM5 as an imaging biomarker for NEPC and other AR$^-$ prostate cancers to expand the diagnostic tools for early detection of these tumors. We investigated ^{89}Zr-labeled labetuzumab as a CEACAM5-targeted PET imaging agent, and we assessed its ability to detect AR$^-$ prostate cancers in vivo.

MATERIALS AND METHODS

Information on cell lines, xenograft establishment, immunohistochemistry, Western blotting, and matrix-assisted laser desorption/ionization determination of chelator-to-antibody ratio can be found in the supplemental materials (available at http://jnm.snmjournals.org). Methods for the analysis of CEACAM5 expression in organoids and metastatic biopsies are also reported in the supplemental materials.

Chemicals

The humanized monoclonal antibody labetuzumab was obtained from Genscript (purity > 99% as confirmed by size-exclusion chromatography–high-performance liquid chromatography; Supplemental Fig. 1). *p*-isothiocyanatobenzoyl DFO was obtained from Macrocyclics. ^{89}Zr was produced by proton bombardment of an ^{89}Y foil on a cyclotron (*20*) and supplied by the Radiochemistry and Molecular Imaging Probes Core at Memorial Sloan Kettering Cancer Center or by 3D Imaging. All aqueous solutions used for conjugation and radiolabeling were prepared with Chelex (Bio-Rad)-treated deionized water.

Conjugation

Conjugation was performed according to literature procedures (*21*). Labetuzumab (Genscript) or IgG1 (InVivoMab BE0297; Bio X Cell) solution in phosphate-buffered saline (PBS) was buffered to pH 8.5–9.0, followed by incubation with a 6-molar excess of the chelator *p*-isothiocyanatobenzoyl-DFO (8 mM in DMSO, <2% total volume) for 90 min on a thermomixer (37°C, 350 rpm). The immunoconjugates were then purified by size-exclusion chromatography on a PD-10 desalting column (GE Healthcare), eluted with PBS, and concentrated with a 50,000 molecular weight cut-off Amicon centrifugal filter.

Radiolabeling

The [^{89}Zr]Zr-oxalate solution (7.4 MBq) was adjusted to pH 6.8–7.2 by the addition of 1 M sodium carbonate (Na_2CO_3) and incubated at 37°C with the DFO-mAbs (labetuzumab-DFO or IgG-DFO isotype-matched control, 20 μg) for 1 h on a thermomixer (37°C, 350 rpm). Radiochemical purity was assessed by silica gel radio–instant thin-layer chromatography using 50 mM ethylenediaminetetraacetic acid as the eluent or by radio–high-performance liquid chromatography with a Yarra SEC-3000 column (Phenomenex) and an isocratic method (flow rate, 1 mL/min) using citrate buffer at pH 6.4 (100 mM sodium citrate, 100 mM sodium chloride) as the mobile phase. The product was purified on a PD-10 desalting column whenever radiochemical purity was inferior to 95%.

Stability to demetallation in serum was evaluated by incubating [^{89}Zr]Zr-DFO-labetuzumab in human serum at 37°C for 5 d. Radiochemical purity at different time points was determined by instant thin-layer chromatography in 50 mM ethylenediaminetetraacetic acid.

Bead-Binding Assay

To determine the CEACAM5 target-binding fraction of [^{89}Zr]Zr-DFO-labetuzumab, a bead-based binding assay was performed (*22*). Briefly, 20 μL of nickel–nitrilotriacetic acid beads (HisPur Beads; Thermo Fisher) were added to each microcentrifuge tube, washed with PBS with Tween (Croda Americas LLC) (PBST) (0.05% polysorbate-20 solution in PBS), and resuspended in 400 μL of PBST. One microgram of His-tagged CEACAM5 (10 μL, 0.1 mg/mL aqueous solution; Thermo Fisher Scientific) was added to each tube, and all tubes were placed on a rotating platform at 4°C for 15 min before centrifugation, removal of the supernatant, and washing with PBST. The beads were then resuspended in 400 μL of PBST, and 1 ng of [^{89}Zr]Zr-DFO-labetuzumab (1 μL of a 1 ng/μL solution in PBST) was added to all tubes. Tubes were left rotating at 4°C for 30 min. The supernatant was then collected, and the beads were washed 3 times with PBST. Beads, supernatant, and washing tubes were measured on a γ-counter, and the percentage of bead-bound activity was calculated. For the control, the procedure was the same except no His-tagged CEACAM5 was added to assess nonspecific binding of [^{89}Zr]Zr-DFO-labetuzumab to the naked beads. For the blocking group, the procedure was the same except for an excess of labetuzumab (5 μg, 5,000× excess), which was added to block specific binding of [^{89}Zr]Zr-DFO-labetuzumab to His-tagged CEACAM5.

Cell-Binding Assay

Cells were harvested, counted, placed in microcentrifuge tubes (10×10^6 cells in 0.2 mL of culture medium), and put on ice. Twenty microliters (3 ng) of a 0.15 μg/mL solution of [^{89}Zr]Zr-DFO-labetuzumab in PBS with 1% bovine serum albumin were added to each tube. For the blocking experiment, an excess of labetuzumab (5,000× excess) was added to the cells immediately before addition of the radiolabeled antibody. The cells were allowed to incubate for 1 h with gentle stirring in a vortex mixer every 15 min to resuspend the cells.

Then, the cells were centrifuged (600*g*, 5 min) and the supernatant collected. The cells were washed 3 times with 1 mL of ice-cold PBS followed by centrifugation (600*g*, 5 min) and removal of the supernatant in separate microcentrifuge tubes. Lastly, the cell pellet, the medium supernatant, and the 3 wash fractions were placed on a γ-counter to determine the percentage of cell-bound radioactivity of [^{89}Zr]Zr-DFO-labetuzumab.

Animal Studies

All animal experiments were approved by the Institutional Animal Care and Use Committee and Research Animal Resource Center at Memorial Sloan Kettering Cancer Center.

Ex Vivo Biodistribution Studies

Biodistribution studies were performed by euthanizing mice (4 per group) at 24, 48, or 120 h after injection with [^{89}Zr]Zr-DFO-labetuzumab (7.4 MBq, 20 μg, 100 μL in PBS) to evaluate the accumulation of the radiotracer in subcutaneous H660, DU145, or LNCaP xenografts.

Organs of interest and the tumor were harvested, weighed, and counted on a γ-counter to determine the accumulation of radioactivity. The percentage injected dose per gram was determined for each sample by normalizing the counts per sample to the total amount of activity injected.

Imaging Studies

PET imaging of mice bearing subcutaneous prostate cancer xenografts was performed. Mice bearing H660, DU145, or LNCaP tumors were intravenously injected with [^{89}Zr]Zr-DFO-labetuzumab or [^{89}Zr]Zr-DFO-IgG (7.4 MBq, 20 μg, 100 μL in PBS). For the blocking studies in H660 and DU145 models, the mice were preinjected with 20- or 10-fold unconjugated labetuzumab, respectively, 1 h before radiotracer administration. The mice were anesthetized with 1%–2% isoflurane, and images were acquired on an Inveon small-animal PET/CT instrument (Siemens) at different time points. After the final imaging time point, the mice were euthanized and ex vivo biodistribution was performed as described above.

Statistical Analysis

Statistical analysis was performed using GraphPad Prism 9.5.1. One-way ANOVA followed by Tukey multiple-comparison testing was used to identify statistically significant differences in organ accumulation between [^{89}Zr]Zr-DFO-labetuzumab at 120 h and the other groups (threshold for significance, $P = 0.05$).

RESULTS

Labetuzumab was conjugated with the DFO by non–site-specific conjugation to lysine residues according to literature procedures (Fig. 1A). Matrix-assisted laser desorption/ionization–time-of-flight

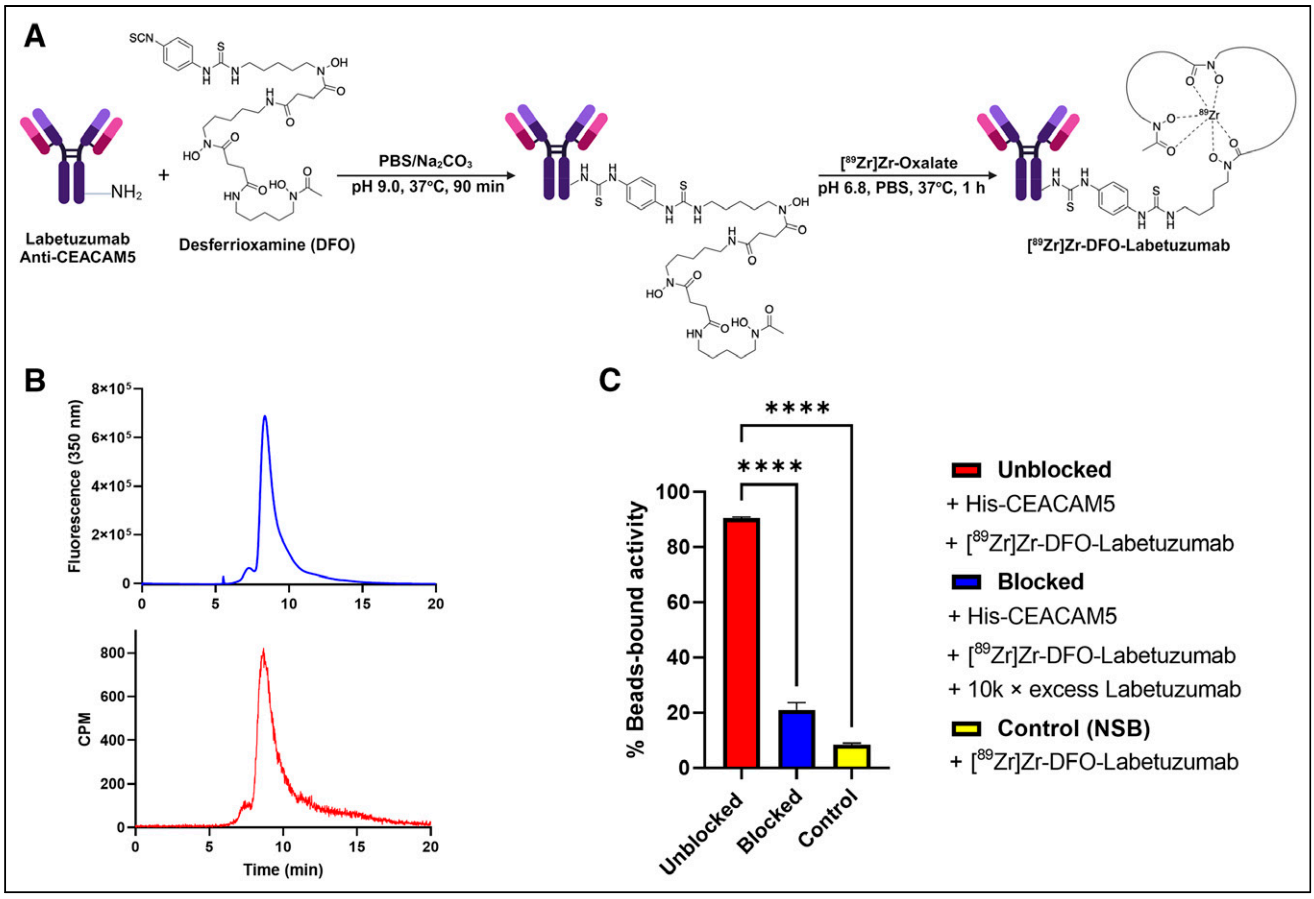

FIGURE 1. Labetuzumab radiolabeling and characterization. (A) Schematic representation of labetuzumab conjugation to DFO-NCS and radiolabeling with ^{89}Zr. (B) Size-exclusion chromatography–high-performance liquid chromatography trace showing quantitative radiolabeling of DFO-labetuzumab conjugate with 1 major peak in radiochromatogram (bottom) corresponding to immunoconjugate peak in fluorescence chromatogram (top, λ emission is 350 nm). The small shoulder at left of main peak is imputable to small amount of immunoconjugate aggregates. (C) Bead-based binding assay confirming CEACAM5-targeting capability of [^{89}Zr]Zr-DFO-labetuzumab, which could be blocked in presence of excess unconjugated antibody (demonstrating specificity) and low nonspecific binding (NSB). Values are expressed as average percentage uptake ± SEM. ****$P < 0.0001$.

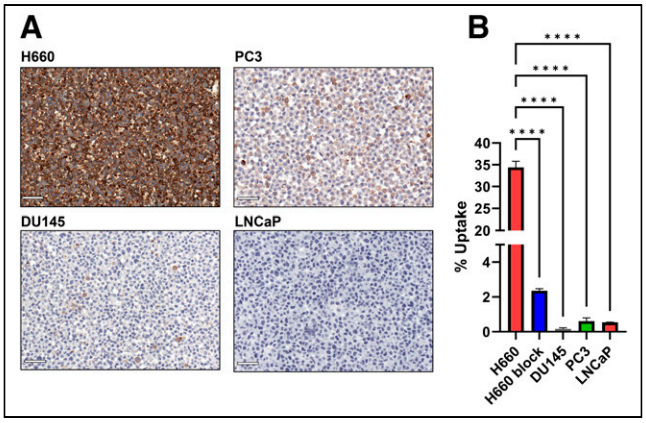

FIGURE 2. In vitro evaluation of prostate cancer cell lines. (A) Immunohistochemistry characterization of CEACAM5 expression in H660, PC3, DU145, and LNCaP cell lines; scale bar is 50 μm. (B) Uptake assay showing selective binding of [^{89}Zr]Zr-DFO-labetuzumab to H660 cells. Values are expressed as average percentage uptake ± SEM. ****$P < 0.0001$.

mass spectrometry analysis of the conjugate (Supplemental Fig. 2) revealed an average of 1.3 chelators per antibody.

Radiolabeling of the immunoconjugate with [^{89}Zr]Zr-oxalate at neutral pH consistently yielded [^{89}Zr]Zr-DFO-labetuzumab in quantitative radiochemical yield (>98%) and purity without the need for purification, as clearly indicated by radio–high-performance liquid chromatography analysis and instant thin-layer chromatography (Fig. 1B; Supplemental Fig. 3). The immunoconjugate remained stable in human serum for up to a week after incubation at 37°C (>98%, Supplemental Fig. 3).

To verify that the labetuzumab antibody maintained binding capacity to CEACAM5 after DFO conjugation and radiolabeling, a bead-binding assay was performed with His-tagged CEACAM5-covered nickel–nitrilotriacetic acid beads. [^{89}Zr]Zr-DFO-labetuzumab retained more than 90% binding to CEACAM5-bearing nickel–nitrilotriacetic acid beads, which could be blocked by an excess of unconjugated labetuzumab (Fig. 1C). These findings confirmed specificity of [^{89}Zr]Zr-DFO-labetuzumab binding to CEACAM5.

Expression of CEACAM5 was investigated in prostate cancer cell lines with a different AR and NEPC status, including hormone-sensitive prostate adenocarcinoma LNCaP (AR-positive [AR$^+$]/neuroendocrine [NE]-negative [NE$^-$]), NEPC H660 (AR$^-$/NE-positive [NE$^+$]), and double-negative prostate cancer (DNPC) DU145 and PC3 (AR$^-$/NE$^-$). Immunohistochemistry analysis of cell pellets showed extremely strong CEA expression in H660 (Fig. 2A). Milder expression was also observed in the DNPC cell lines PC3 and DU145, which are AR-null but do not display NEPC features, whereas AR$^+$ LNCaP cells did not show any CEACAM5 expression (Fig. 2A). On the other hand, when Western blotting was used to measure CEACAM5 protein expression in the same cell lines, only H660 showed visible CEACAM5 expression (Supplemental Fig. 4).

In agreement with these results, a cell-binding assay using [^{89}Zr]Zr-DFO-labetuzumab confirmed high binding to H660 cells (34.3% uptake, Fig. 2B). The binding could be blocked in the presence of excess unlabeled labetuzumab, confirming [^{89}Zr]Zr-DFO-labetuzumab binding specificity to the target antigen. Negligible binding was observed in all the other cell lines.

We then moved to in vivo PET imaging to evaluate the ability of [^{89}Zr]Zr-DFO-labetuzumab to delineate NEPC tumors in male nude mice bearing H660 xenografts. [^{89}Zr]Zr-DFO-labetuzumab showed excellent accumulation in H660 xenografts as early as 24 h and was able to reach remarkable uptake levels at 120 h, demonstrating the potential of anti-CEA imaging in NEPC tumors (Fig. 3A). This was also confirmed by [^{89}Zr]Zr-DFO-labetuzumab biodistribution studies at different time points (Fig. 3B; Supplemental Fig. 5). In contrast, when the [^{89}Zr]Zr-DFO-IgG was used, only low, nonspecific uptake was visible in the H660 tumors at all time points considered (Supplemental Fig. 6). Terminal ex vivo biodistribution (Fig. 3B) for [^{89}Zr]Zr-DFO-IgG similarly showed markedly reduced tumor accumulation compared with [^{89}Zr]Zr-DFO-labetuzumab, whereas uptake in other organs was largely identical, except for the liver, which showed increased uptake for the isotype-matched imaging group.

We further verified the specificity of our tracer in H660 tumors by performing a blocking experiment in which the administration of [^{89}Zr]Zr-DFO-labetuzumab was preceded by injection of excess unlabeled labetuzumab. Lower tumor uptake was observed at all time points, consistent with the specificity of the radioimmunoconjugate for the CEACAM5 receptor (Fig. 3A; Supplemental Fig. 7). Terminal biodistribution (120 h) for the blocking cohort revealed similar accumulation of [^{89}Zr]Zr-DFO-labetuzumab in all organs, with the only significant difference being tumor uptake (Fig. 3B; Supplemental Fig. 5).

On the basis of in vitro results, the AR$^-$/NE$^-$ prostate cancer model DU145 was initially chosen as the negative model for the in vivo study. However, PET imaging and ex vivo biodistribution showed unexpected tumor uptake, although lower than what observed in the H660 model (Figs. 4A and 4B; Supplemental Fig. 8). A blocking experiment with excess unlabeled labetuzumab confirmed that the observed uptake was specific (Fig. 4A; Supplemental Fig. 9). In contrast, when mice bearing subcutaneous AR$^+$/NE$^-$ LNCaP tumors were imaged with [^{89}Zr]Zr-DFO-labetuzumab, little tumor uptake was observed at any time point (Fig. 5; Supplemental Fig. 10).

Accordingly, when the biodistribution in the 3 models was compared (Fig. 6A), the AR$^-$/NE$^+$ H660 xenograft displayed the highest tumor-to-tissue ratios (tumor-to-blood ratio of 11 ± 1, tumor-to-muscle ratio of 98 ± 17), the AR$^-$/NE$^-$ DU145 displayed moderate but specific uptake, and no specific uptake was observed in the AR$^+$/NE$^-$ LNCaP tumors. Image quantification of tumor uptake from the PET study (Supplemental Fig. 11) also showed the same trend. Immunohistochemical analysis of resected tumor samples for each xenograft model (Fig. 6B, isotype-matched control in Supplemental Fig. 12) confirmed our in vivo findings, with H660 xenograft sections showing intense CEACAM5 expression throughout the tissue, DU145 showing heterogeneous CEACAM5 expression, and LNCaP xenografts completely lacking expression.

To check whether our unexpected observation of in vivo expression of CEACAM5 in both AR$^-$/NE$^+$ and AR$^-$/NE$^-$ prostate cancer xenografts is clinically valid and relevant, we analyzed CEACAM5 expression in a large cohort of human tumor organoids and metastatic biopsy samples of prostate cancer previously validated in the literature (*24,25*). In organoid samples (Fig. 7A), we found elevated CEACAM5 transcript levels in both NEPC organoids and a subset of DNPC organoids that the authors classified as stem cell-like prostate cancer, which express CD44 and other stem cell-like markers (*23*). In this classification, DU145 and PC3 are classified as stem cell-like prostate cancers. Generally, organoid expression of CEACAM5 showed a slightly negative correlation with the expression of PSMA, prostate-specific antigen, and AR (Supplemental Fig. 13). For the biopsy samples (Fig. 7B), all tissues displaying CEACAM5 expression (based on single-cell RNA

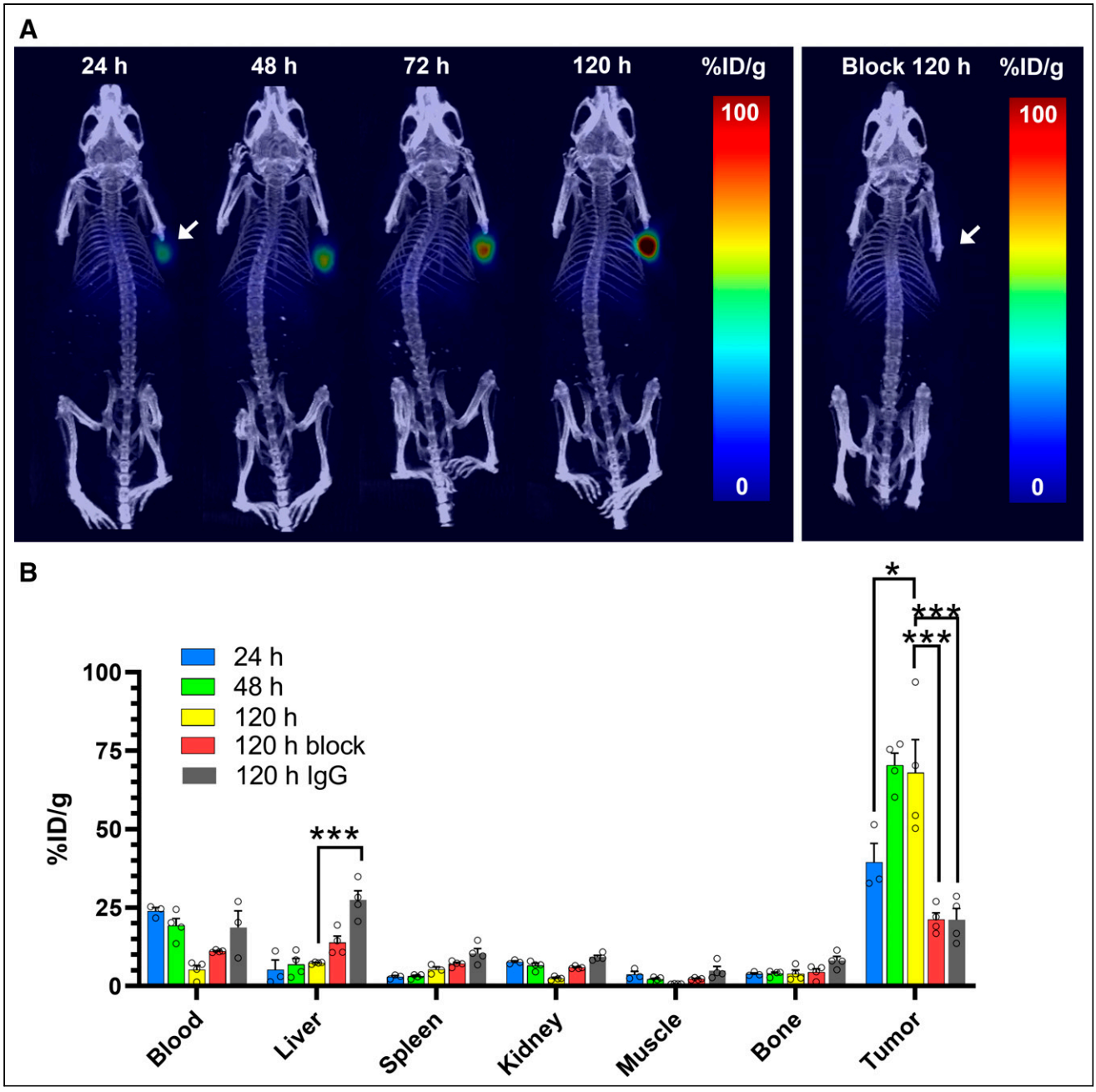

FIGURE 3. Evaluation of [^{89}Zr]Zr-DFO-labetuzumab in H660 xenografts. (A) Exemplar maximum-intensity projections obtained by dynamic PET imaging of mice injected with [^{89}Zr]Zr-DFO-labetuzumab at different time points after administration, showing remarkably high uptake of radioimmunoconjugate. This is compared (on right) with negligible uptake obtained at 120 h when excess of unconjugated labetuzumab was administered 1 h before [^{89}Zr]Zr-DFO-labetuzumab, confirming specific tumor uptake. (B) Ex vivo biodistribution in selected organs comparing accumulation of [^{89}Zr]Zr-DFO-labetuzumab at different time points, with the same tracer in presence of excess labetuzumab and [^{89}Zr]Zr-DFO-IgG. Values are expressed as average percentage injected dose per gram (%ID/g) ± SEM ($n = 4$, full biodistribution data in Supplemental Fig. 5). *$P < 0.05$. ***$P < 0.005$.

sequencing) were consistently located within the AR$^-$/NE$^+$ (NEPC) or the AR$^-$/NE$^-$ (DNPC) clusters, as classified according to the Uniform Manifold Approximation and Projection (Supplemental Fig. 14), but not in AR$^+$ castration-resistant prostate cancer cluster.

DISCUSSION

Receptor-targeted PET imaging provides a noninvasive tool to identify prostate cancer lesions, even when these are relatively inaccessible to biopsy, such as bone metastases. Compared with biopsy, imaging enables a better understanding of tumor and intratumor heterogeneity, by essentially illustrating the expression of a specific target receptor in the tumor tissue. Although PET imaging biomarkers have been identified and translated into the clinic for AR$^+$ prostate cancer (most notably ^{18}F-/^{68}Ga-PSMA), currently there are no clinical diagnostic tools for NEPC and DNPC.

The cell-adhesion molecule CEACAM5 has been investigated for imaging of colorectal cancer and, to a lesser extent, non–small cell

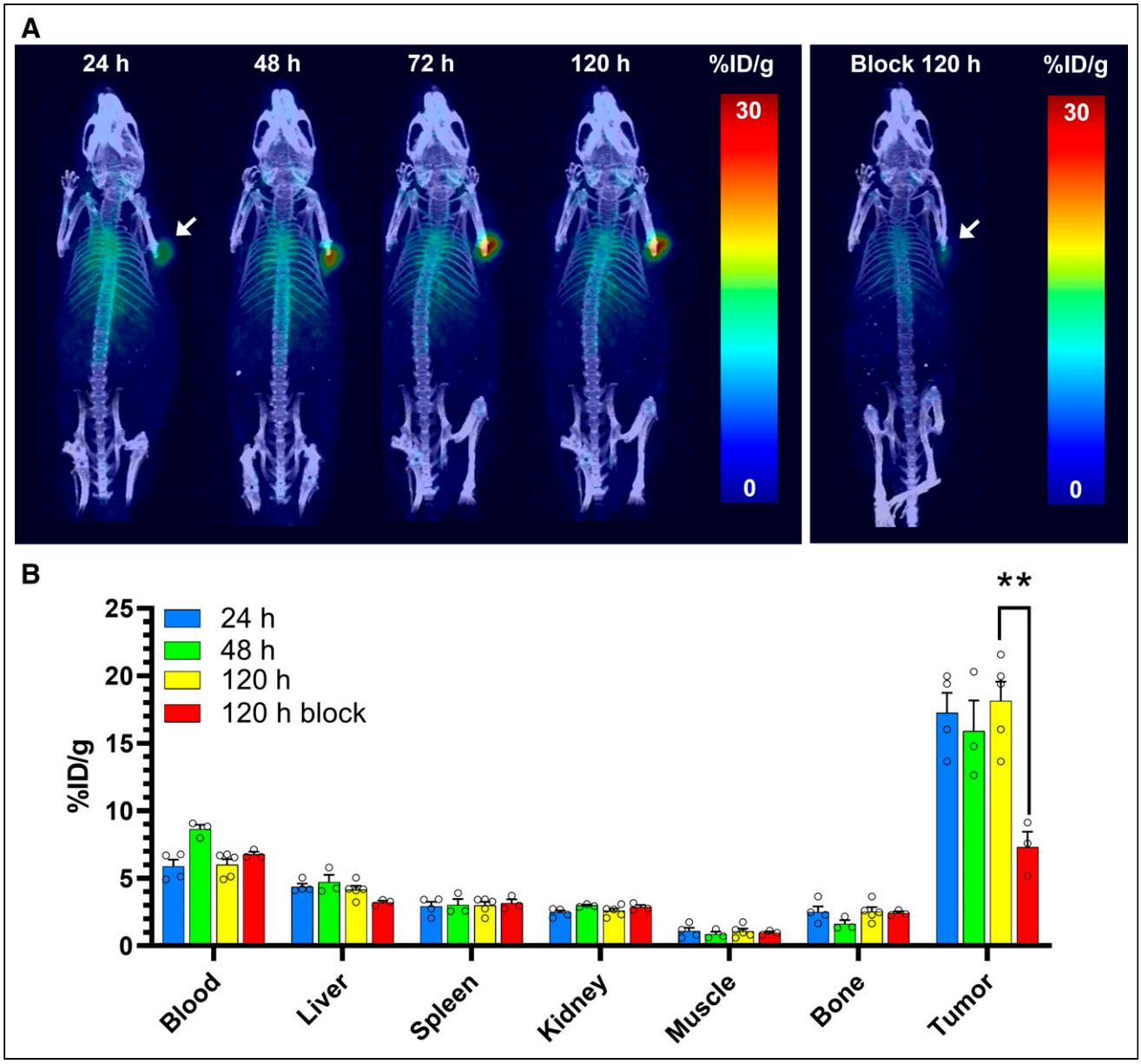

FIGURE 4. Evaluation of [^{89}Zr]Zr-DFO-labetuzumab in DU145 xenografts. (A) Exemplar maximum-intensity projections obtained by dynamic PET imaging of mice injected with [^{89}Zr]Zr-DFO-labetuzumab at different time points after administration, compared (on right) with negligible uptake obtained at 120 h for blocking study. (B) Ex vivo biodistribution in selected organs comparing accumulation of [^{89}Zr]Zr-DFO-labetuzumab at different time points with and without blocking. Values are expressed as average percentage injected dose per gram (%ID/g) ± SEM ($n = 4$, full biodistribution data in Supplemental Fig. 8). $^{**}P < 0.01$.

lung cancer. More recently, CEACAM5 was identified as a key receptor in NEPC, with the CEACAM5-targeting antibody–drug conjugate labetuzumab govitecan showing strong antitumor activity in preclinical studies with NEPC models (*18*).

Here, we have investigated the ability of [^{89}Zr]Zr-DFO-labetuzumab to effectively delineate NEPC in vivo using PET imaging in a H660 xenograft model, which we have previously shown to express the NEPC marker synaptophysin while lacking common prostate cancer biomarkers (AR, prostate-specific antigen, and PSMA) (*7*). The PET images obtained using [^{89}Zr]Zr-DFO-labetuzumab in this model demonstrated the remarkable ability of the radiotracer to accumulate in H660 xenografts. Specificity of the CEACAM5 targeting was confirmed by the ability of excess unlabeled labetuzumab to block tumor accumulation of the radiotracer and by the negligible tumor uptake of the ^{89}Zr-labeled isotype-matched control.

Intriguingly, the AR$^-$/NE$^-$ prostate cancer model DU145 could also be effectively delineated with [^{89}Zr]Zr-DFO-labetuzumab in vivo, and although much lower tumor accumulation was observed, contrast remained high because of low background signal. Immunohistochemical characterization of DU145 cells and xenograft showed that, although little expression of CEACAM5 was detected in cells, moderate levels of expression were measured in vivo. Previous reports by DeLucia et al. (*18*) and Lee et al. (*8*) have used the DU145 cells as a negative control but did not explore their behavior in vivo. Using PET imaging, we could gain unique

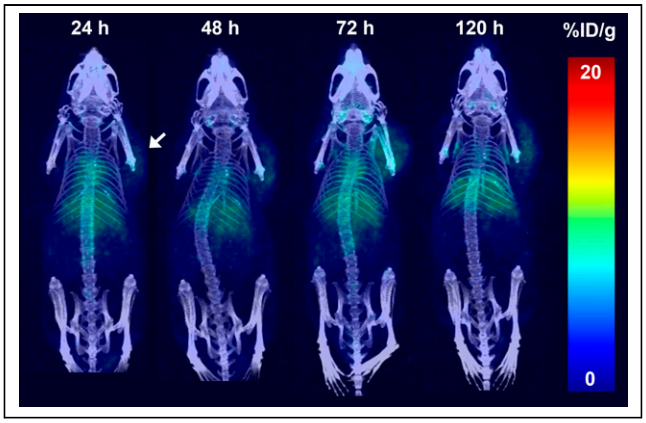

FIGURE 5. Evaluation of [^{89}Zr]Zr-DFO-labetuzumab in LNCaP xenografts. Exemplar maximum-intensity projections were obtained by dynamic PET imaging of LNCaP-bearing mice injected with [^{89}Zr]Zr-DFO-labetuzumab at different time points after administration (ex vivo biodistribution data in Supplemental Fig. 10).

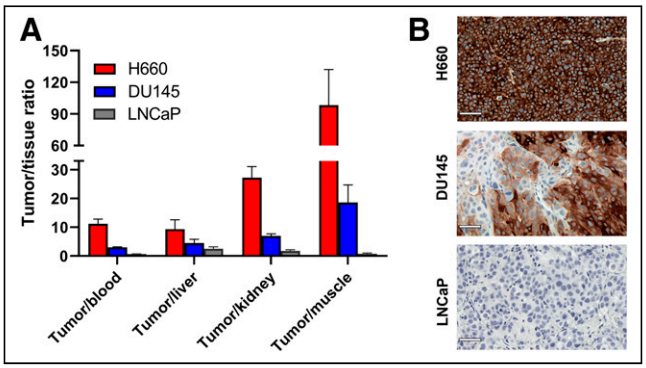

FIGURE 6. (A) Comparison of tumor-to-tissue ratios of [^{89}Zr]Zr-DFO-labetuzumab accumulation at 120 h after injection in 3 different xenograft models. (B) Ex vivo immunohistochemistry showing CEACAM5 expression in 3 models (scale bar, 50 μm).

insight suggesting that DU145 xenografts interact with the tumor microenvironment and start expressing CEACAM5.

Remarkably, analysis of CEACAM5 expression in human organoids and metastatic biopsy samples (Fig. 7) validated our experimental observation that CEACAM5 is expressed in both NEPC and a subset of DNPC prostate cancer. Our data and the literature reports suggest that CEACAM5 could serve as a biomarker for diagnosis of different types of AR$^-$ prostate cancer. This is particularly relevant because the increased use of potent AR signaling inhibitors in patients is resulting in a significantly increased proportion of patients with AR$^-$ prostate cancer of both NE$^-$ and NE$^+$ subtypes compared with the traditional AR$^+$ phenotype (*2*). For these patients, the development of an AR$^-$ diagnostic tool, such as CEACAM5-targeted immuno-PET, could enable early diagnosis and inform treatment decisions in the same way as PSMA PET does for AR-dependent prostate cancer.

One inherent limitation of our study, in view of a potential clinical translation, is the absence of CEACAM5 expression in mouse tissue, which prevents us from predicting specific accumulation of the radiotracer in nontarget organs. However, previous clinical imaging studies with anti-CEACAM5 antibodies have shown a relatively low background for this target (*25,26*). Another limitation of our study is that it is limited to subcutaneous xenograft tumors, which may not be representative of clinical AR$^-$ lesions. Further studies will include imaging in patient-derived xenograft models previously determined to be AR$^-$ by immunohistochemistry. Finally, to enable imaging at earlier time points than is possible with directly labeled anti-CEACAM5 full-length antibodies, pretargeting strategies (*27*) or smaller formats such as single-domain antibodies (*16*) could be explored in future studies.

Importantly, besides its potential as a diagnostic tool for AR$^-$ prostate cancer, PET imaging with [^{89}Zr]Zr-DFO-labetuzumab could also be used for patient stratification. Here, CEACAM5 immuno-PET imaging would serve as a biomarker to identify prostate cancer patients who could benefit from labetuzumab-govitecan and other CEACAM5-targeted therapies, including targeted radiotherapy approaches based on the same antibody carrying β- and α-emitting radiometals.

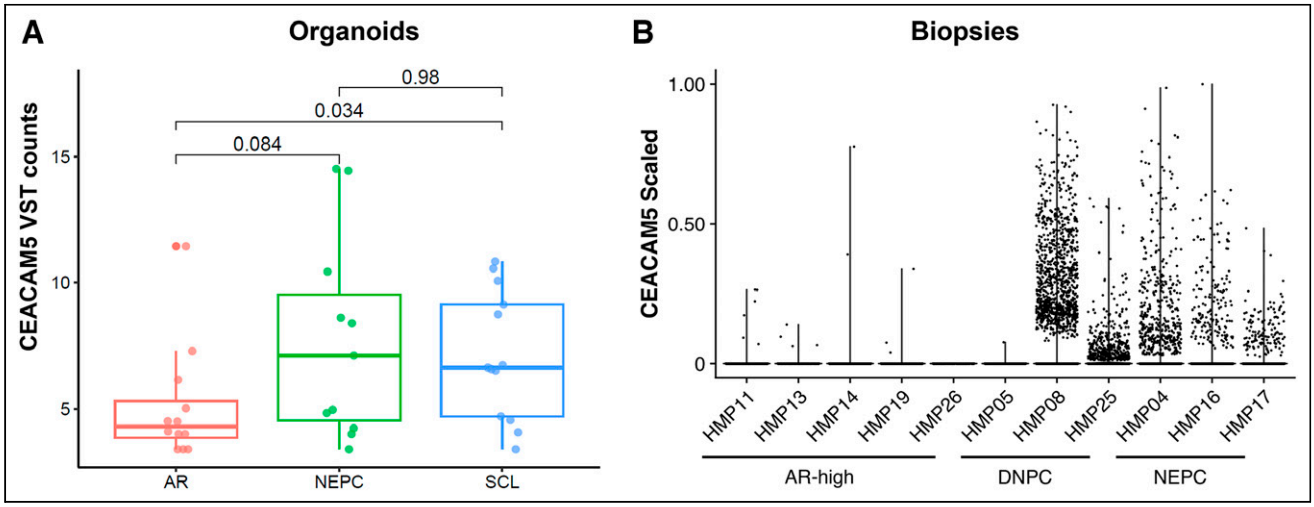

FIGURE 7. Evaluation of CEACAM5 expression in prostate cancer organoids and biopsies. (A) Box plots showing variance-stabilized transformed (VST) counts of CEACAM5 in AR$^+$, NEPC, and stem cell-like (SCL) organoid subtypes (significance analysis by Wilcox test). (B) Minimum to maximum scaled CECAM5 expression plotted by tumor biopsy and labeled by AR-high, DNPC, and NEPC biopsies.

CONCLUSION

Overall, these data show the ability of CEACAM5-targeted immuno-PET imaging to clearly delineate NEPC and other AR^- prostate cancers in vivo and pave the way to the development of an imaging-based diagnostic tool to enable early detection of these lesions and inform patient treatment.

DISCLOSURE

The study was supported by NCI R35 CA232130 (Jason Lewis), NIH T32 GM073546 (Joshua Korsen and Tran Hoang), and the Prostate Cancer Foundation (Jason Lewis). We acknowledge the Radiochemistry and Molecular Imaging Probes Core Facility, the Small Animal Imaging Facility, and the Molecular Cytology Core Facility at Memorial Sloan Kettering, which are supported by NIH grant P30 CA08748. No other potential conflict of interest relevant to this article was reported.

KEY POINTS

QUESTION: Can CEACAM5-targeted immuno-PET identify AR-null tumors, specifically NEPC, in vivo?

PERTINENT FINDINGS: [^{89}Zr]Zr-DFO-labetuzumab was able to clearly delineate the NE^+/AR^- model H660 in vivo but also, although to a lesser extent, the NE^-/AR^- model DU145. No uptake of the radiotracer was observed in NE^-/AR^+ LNCaP xenografts, suggesting its selectivity for AR^- prostate cancer.

IMPLICATIONS FOR PATIENT CARE: CEACAM5-targeted immuno-PET has the potential to be translated clinically as a noninvasive diagnostic tool to enable early detection of AR^- prostate cancer.

REFERENCES

1. Key statistics for prostate cancer. American Cancer Society website. https://www.cancer.org/cancer/types/prostate-cancer/about/key-statistics. Accessed April 24, 2024.
2. Bluemn EG, Coleman IM, Lucas JM, et al. Androgen receptor pathway-independent prostate cancer is sustained through FGF signaling. *Cancer Cell.* 2017;32:474–489.e6.
3. Roberts MJ, Maurer T, Perera M, et al. Using PSMA imaging for prognostication in localized and advanced prostate cancer. *Nat Rev Urol.* 2023;20:23–47.
4. Watson PA, Arora VK, Sawyers CL. Emerging mechanisms of resistance to androgen receptor inhibitors in prostate cancer. *Nat Rev Cancer.* 2015;15:701–711.
5. Merkens L, Sailer V, Lessel D. Aggressive variants of prostate cancer: underlying mechanisms of neuroendocrine transdifferentiation. *J Exp Clin Cancer Res.* 2022;41:46.
6. Korsen JA, Kalidindi TM, Khitrov S, et al. Molecular imaging of neuroendocrine prostate cancer by targeting Delta-like ligand 3. *J Nucl Med.* 2022;63:1401–1407.
7. Korsen JA, Gutierrez JA, Tully KM, et al. Delta-like ligand 3-targeted radioimmunotherapy for neuroendocrine prostate cancer. *Proc Natl Acad Sci USA.* 2022;119:e2203820119.
8. Lee JK, Bangayan NJ, Chai T, et al. Systemic surfaceome profiling identifies target antigens for immune-based therapy in subtypes of advanced prostate cancer. *Proc Natl Acad Sci USA.* 2018;115:E4473–E4482.
9. Aparicio AM, Harstark AL, Corn PG, et al. Platinum-based chemotherapy for variant castrate-resistant prostate cancer. *Clin Cancer Res.* 2013;19:3621–3630.
10. Kuespert K, Pils S, Hauck CR. CEACAMs: their role in physiology and pathophysiology. *Curr Opin Cell Biol.* 2006;18:565–571.
11. Paxton RJ, Mooser G, Pande H, et al. Sequence analysis of carcinoembryonic antigen: identification of glycosylation sites and homology with the immunoglobulin supergene family. *Proc Natl Acad Sci USA.* 1987;84:920–924.
12. Beauchemin N, Arabzadeh A. Carcinoembryonic antigen-related cell adhesion molecules (CEACAMs) in cancer progression and metastasis. *Cancer Metastasis Rev.* 2013;32:643–671.
13. Gold P, Freedman SO. Specific carcinoembryonic antigens of the human digestive system. *J Exp Med.* 1965;122:467–481.
14. Shively JE, Beatty JD. CEA-related antigens: molecular biology and clinical significance. *Crit Rev Oncol Hematol.* 1985;2:355–399.
15. Akhavan D, Yazaki P, Yamauchi D, et al. Phase I study of yttrium-90 radiolabeled M5A anti-carcinoembryonic antigen humanized antibody in patients with advanced carcinoembryonic antigen producing malignancies. *Cancer Biother Radiopharm.* 2020;35:10–15.
16. Li L, Lin XF, Wang L, et al. Immuno-PET of colorectal cancer with a CEA-targeted [^{68}Ga]Ga-nanobody: from bench to bedside. *Eur J Nucl Med Mol Imaging.* 2023;50:3735–3749.
17. Blumenthal RD, Leon E, Hansen HJ, Goldenberg DM. Expression patterns of CEACAM5 and CEACAM6 in primary and metastatic cancers. *BMC Cancer.* 2007;7:2.
18. DeLucia DC, Cardillo TM, Ang L, et al. Regulation of CEACAM5 and therapeutic efficacy of an anti-CEACAM5-SN38 antibody-drug conjugate in neuroendocrine prostate cancer. *Clin Cancer Res.* 2021;27:759–774.
19. Kim YJ, Li W, Zhelev DV, et al. Chimeric antigen receptor-T cells are effective against CEACAM5 expressing non-small cell lung cancer cells resistant to antibody-drug conjugates. *Front Oncol.* 2023;13:1124039.
20. Holland JP, Sheh YC, Lewis JS. Standardized methods for the production of high specific-activity zirconium-89. *Nucl Med Biol.* 2009;36:729–739.
21. Cooper MS, Sabbah E, Mather SJ. Conjugation of chelating agents to proteins and radiolabeling with trivalent metallic isotopes. *Nat Protoc.* 2006;1:314–317.
22. Sharma SK, Lyashchenko SK, Park HA, et al. A rapid bead-based radioligand binding assay for the determination of target-binding fraction and quality control of radiopharmaceuticals. *Nucl Med Biol.* 2019;71:32–38.
23. Tang FY, Xu D, Wang SQ, et al. Chromatin profiles classify castration-resistant prostate cancers suggesting therapeutic targets. *Science.* 2022;376:eabe1505.
24. Chan JM, Zaidi S, Love JR, et al. Lineage plasticity in prostate cancer depends on JAK/STAT inflammatory signaling. *Science.* 2022;377:1180–1191.
25. Wong JY, Yamauchi DM, Adhikarla V, et al. First-in-human pilot PET immunoimaging study of Cu-64-anti-carcinoembryonic antigen monoclonal antibody (hT84.66-M5A) in patients with carcinoembryonic antigen-producing cancers. *Cancer Biother Radiopharm.* 2023;38:26–37.
26. Wong JY, Thomas GE, Yamauchi D, et al. Clinical evaluation of indium-111-labeled chimeric antiCEA monoclonal antibody. *J Nucl Med.* 1997;38:1951–1959.
27. Bodet-Milin C, Bailly C, Touchefeu Y, et al. Clinical results in medullary thyroid carcinoma suggest high potential of pretargeted immuno-PET for tumor imaging and theranostic approaches. *Front Med (Lausanne).* 2019:6:124.